Journal of Geophysical Research: Solid Earth

Supporting Information for

Optimizing sensor configurations for the detection of slow slip earthquakes in seafloor pressure records, using the Cascadia Subduction Zone as a case study

Erik K. Fredrickson[1], William S. D. Wilcock[1], David A. Schmidt[2], Parker MacCready[1], Emily Roland[1], Alexander L. Kurapov[3], Mark A. Zumberge[4], Glenn S. Sasagawa[4]

[1]School of Oceanography, University of Washington, Seattle, Washington, USA. [2]Department of Earth and Space Sciences, University of Washington, Seattle, Washington, USA. [3]Coast Survey Development Laboratory, National Oceanic and Atmospheric Administration, Silver Spring, Maryland, USA. [4]Institute of Geophysics and Planetary Physics, Scripps Institution of Oceanography, University of California, San Diego, La Jolla, California, USA

Contents of this file

Introduction

The included materials provide detailed information about the pressure data used in our analysis, our processing of those pressure data, and the comparability of the two oceanographic models. We also present additional figures of slow slip modeling scenarios discussed in the main text.

Text S1.

In each year there are pressure records with significant quality issues that render the data unusable for this study. These issues include off-scale/flatline output and the presence of high-amplitude, long-period signals, that could not realistically be produced at the seafloor. Additionally, in the 2013-2014 experiment year, there were systematic mechanical failures in all but one of the pressure sensors, possibly related to air bubbles in the oil-filled inlet tubing (personal communication, Andrew Barclay, Lamont-Doherty Earth Observatory), that lead to increased noise across all frequencies above 0.02 day^{-1} and unpredictable response to pressure perturbations. A single pressure sensor is not sufficient to detect a SSE so we exclude this year from this study. In the 2014-2015 experiment year, 5 instruments yielded pressure data of

higher amplitude and increased high-frequency noise relative to instruments from similar locations in this and previous years. This may be due to residual mechanical issues with the sensors and we exclude these data in our assessment of oceanographic signal reduction.

Data from the OOI cabled array came online in 2014 and include 2 high-resolution APG instruments on the margin, all Sea-Bird devices utilizing Paroscientific sensors, which are used to supplement the final year of CI data. A series of seafloor pressure benchmarks with Paroscientific APGs were deployed in 2014 and 2015 across the margin offshore central Oregon as part of an ongoing interseismic deformation experiment (Cook et al., 2017). Data from one of these benchmarks spans the final year of the CI experiment and is included in our analysis.

Text S2.

The pressure data used in this study are corrected with a 3rd order polynomial, modeled using least-squares, to eliminate instrument drift and long period (i.e. seasonal) oceanographic signals. We elected to use a third-order polynomial after examining the effects of correcting with polynomials order 1-5 as well as a linear trend with an initial exponential, all fit by least squares. A third-order polynomial is the lower order polynomial that successfully removes annual signals that are apparent in much of the data. Some examples of pressure differences from records fit in these ways are shown in Figure S1. We determined that a polynomial of 3rd order was the best tradeoff between RMS reduction and avoiding over-fitting the data. Our results are not sensitive to the use of higher-order polynomials.

Text S3.

Individual pressure records of the LiveOcean and WCOFS oceanographic models are compared at continental shelf, slope, and abyssal plain locations for the 2013-2014 year in time (Figure S2a-c) and frequency space (Figure S2c-f). The models show the best agreement on or near the continental shelf (Figure S2a,d), where the amplitude spectra are broadly comparable and signals are similarly resolved in either model. On the abyssal plain (Figure S2c,f), the amplitude spectra remain comparable, but the timing and amplitude of pressure signals do not show good agreement between models. Continental slope locations (Figure S2b,e) fall somewhere between the two, with the most large-amplitude, low-frequency signals similarly resolved but higher-frequency signals varying.

The bottom pressure RMS are highly similar between the two models (Figure S3a,b), as are the difference RMS (Figure S3c,d). The LiveOcean model generally predicts higher amplitude signals on the inner continental shelf and slightly lower amplitudes on the slope and abyssal plain. Also, the WCOFS model features a region of low RMS near the shelf break not seen in the LiveOcean model. Similarly, difference RMS of the LiveOcean model are larger on the inner continental shelf, but otherwise the two models predict very similar difference amplitudes. The RMS change obtained by subtracting the WCOFS model from LiveOcean at each location within their common domain is contoured in Figure S4a. Signal amplitudes are reduced near the coast but are unchanged elsewhere, with the exception of a >0.5 cm increase seen near the shelf break and for a small subset of the abyssal plain. Figure S4b contours the R^2 of the fit (equation 1) of the WCOFS model to the LiveOcean model. Most locations show $R^2 > 0.2$, with values as large as 0.75 on the inner continental shelf, while select abyssal plain locations and locations near the shelf break show $R^2 < 0$ and as low as -0.6.

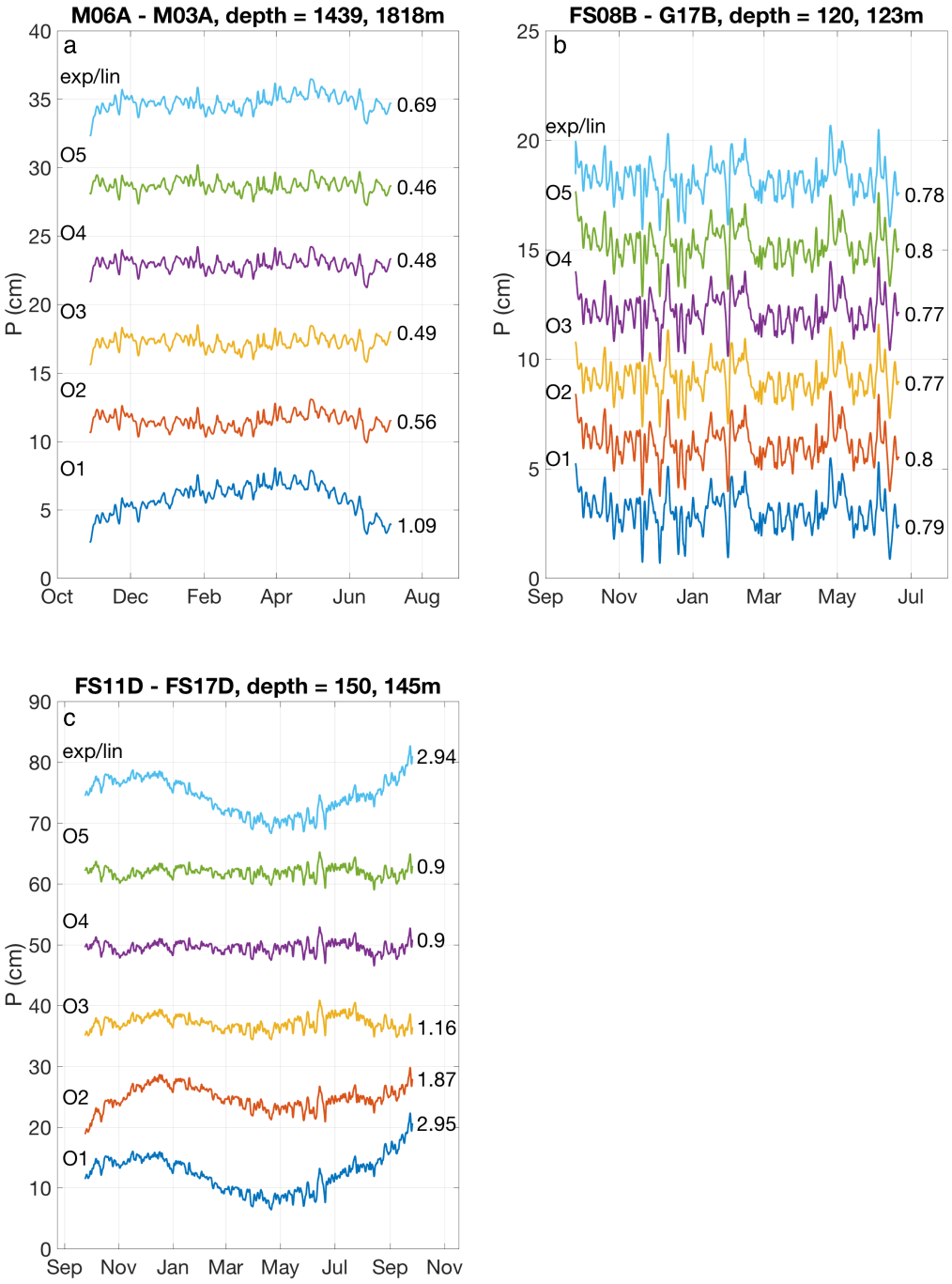

Figure S1. Comparison of methods for removing instrument drift for three example pressure differences. From bottom to top, pressure differences were corrected with a polynomial fit of order 1-5 and with a combination linear and exponential fit. Traces are offset for display purposes and RMS values (in cm) are reported next to each. (a) Instruments from the 2011-2012 year on the lower continental slope. (b) Instruments from the 2012-2013 year on the continental shelf. (c) Instruments from the 2014-2015 year on the continental shelf.

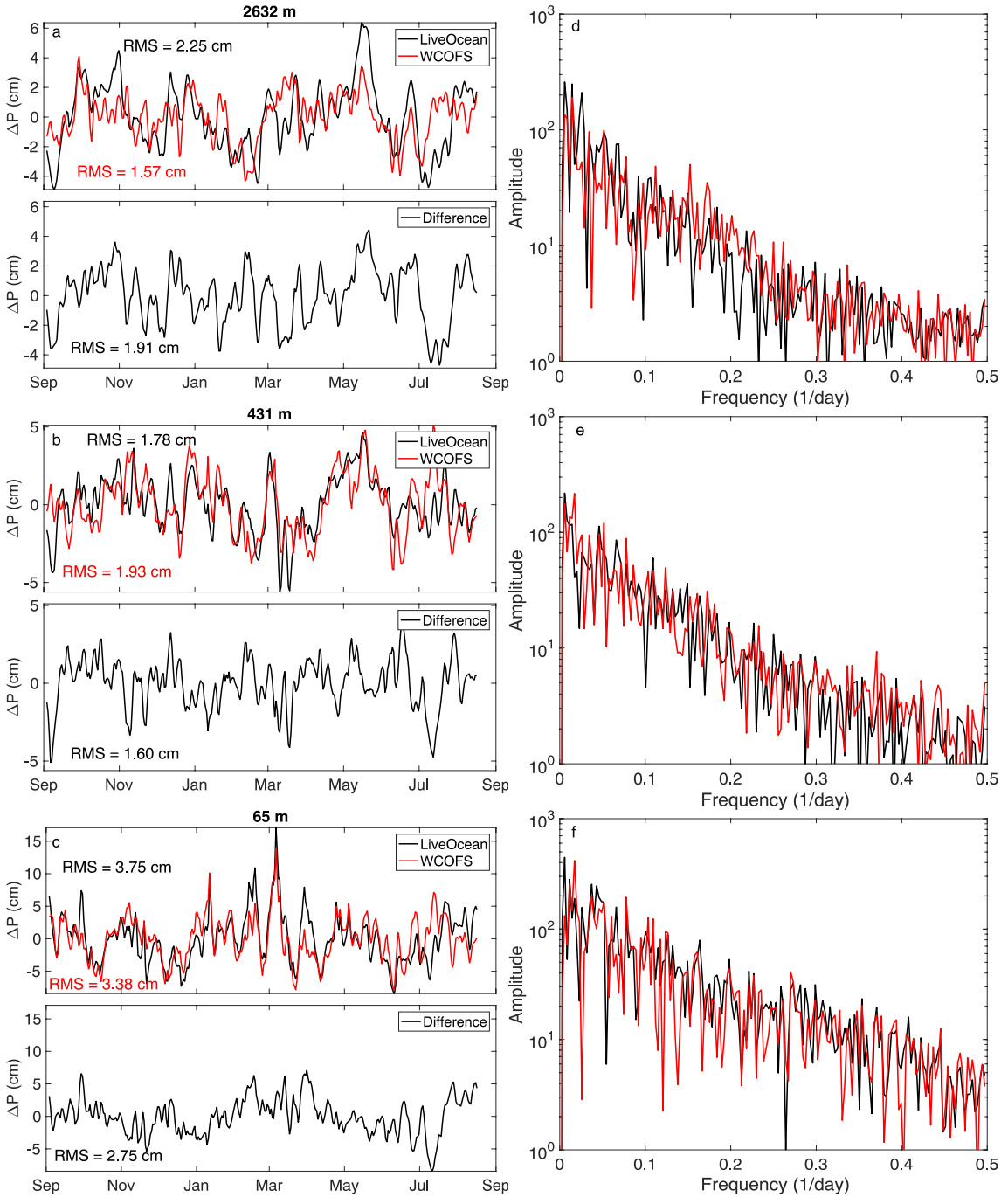

Figure S2. Comparison of WCOFS and LiveOcean models in 2013-2014, when the models overlap, for the locations in Figure 6b-d. As with the APG data, these pressures are tidally filtered with a 24-24-25 Godin filter (Godin, 1972). (a-c) Bottom pressure timeseries (upper panels) and differences (lower panels) for a continental shelf, slope, and abyssal plain location. (d-f) Amplitude spectra of the timeseries at the same locations.

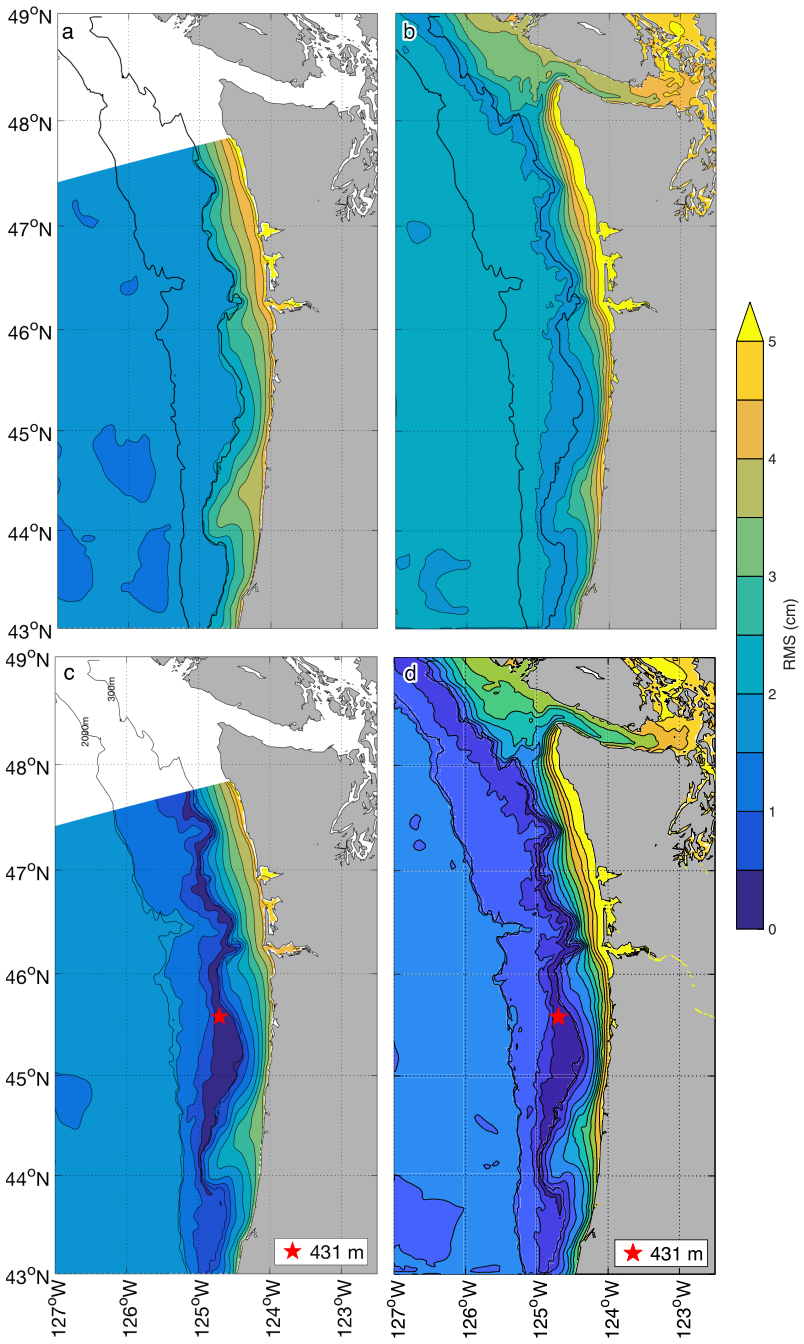

Figure S3. Comparison of the seafloor pressure output from the WCOFS and Live Ocean circulation models. (a) Contours of bottom pressure RMS for 2013-2014 for the WCOFS model, with a Godin 24-24-25 filter (Godin, 1972) applied and a 3rd order polynomial fit removed. (b) Contours of RMS for the 2013-2014 LiveOcean model, processed the same way. (c) Contours of pressure difference RMS against a reference location at 500 m depth, as indicated by the red star, from the WCOFS model. (d) Contours of pressure difference RMS from the LiveOcean model, for the same reference location. Black lines show the 300 m and 2000 m isobaths.

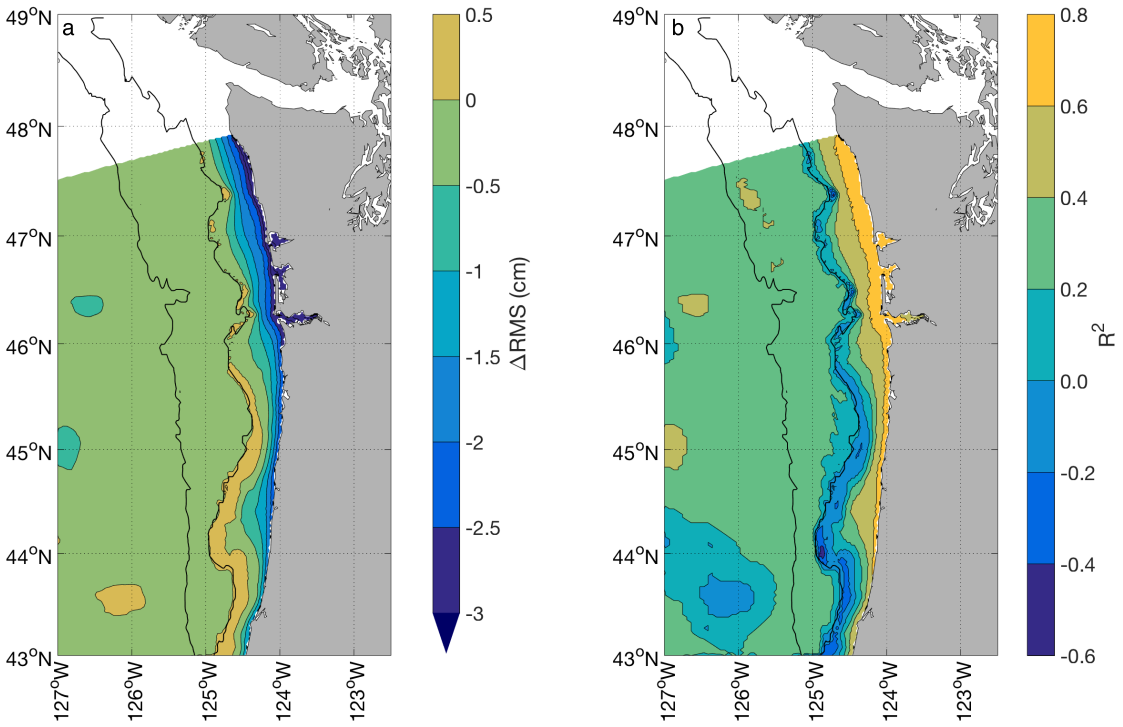

Figure S4. (a) Contours of change in bottom pressure RMS when subtracting the WCOFS model from the LiveOcean model, after applying to both a Godin 24-24-25 filter (Godin, 1972) and removing a 3rd order polynomial fit. (b) Contours of the R^2 of the fit of the WCOFS model to the LiveOcean model for every location in their shared domain. Black lines show the 300 m and 2000 m isobaths.

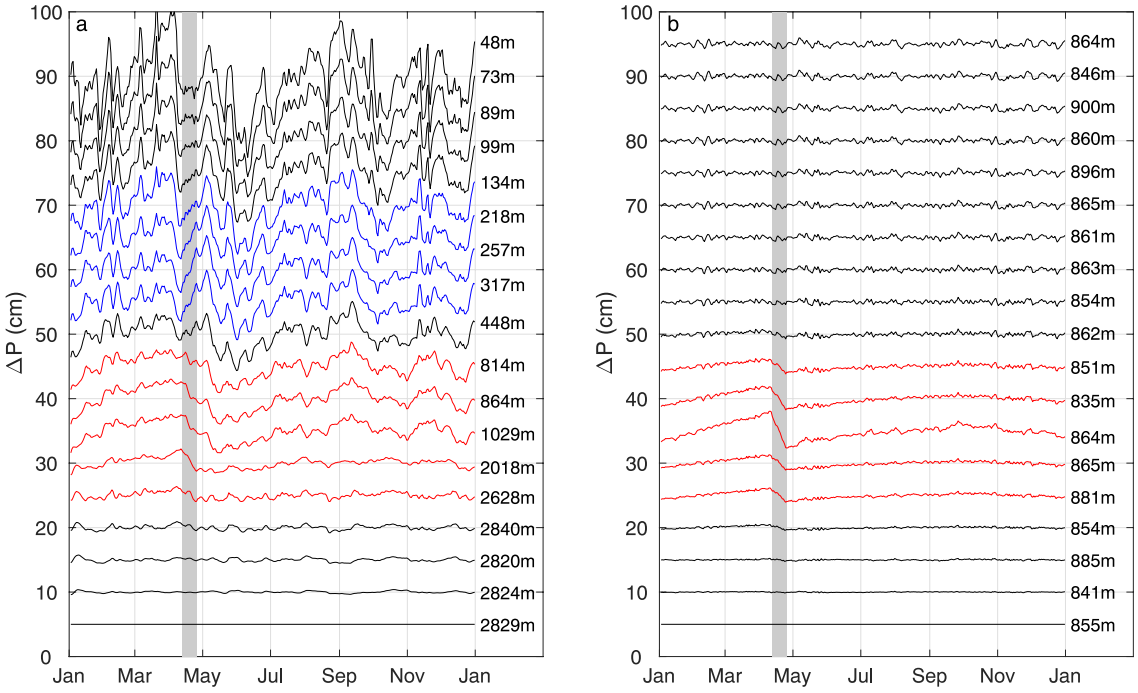

Figure S5. As for Figure 9, but for an earlier onset time of the SSE, now beginning on 12 April 2013. (a) As for Figure 9b. (b) As for Figure 9c.

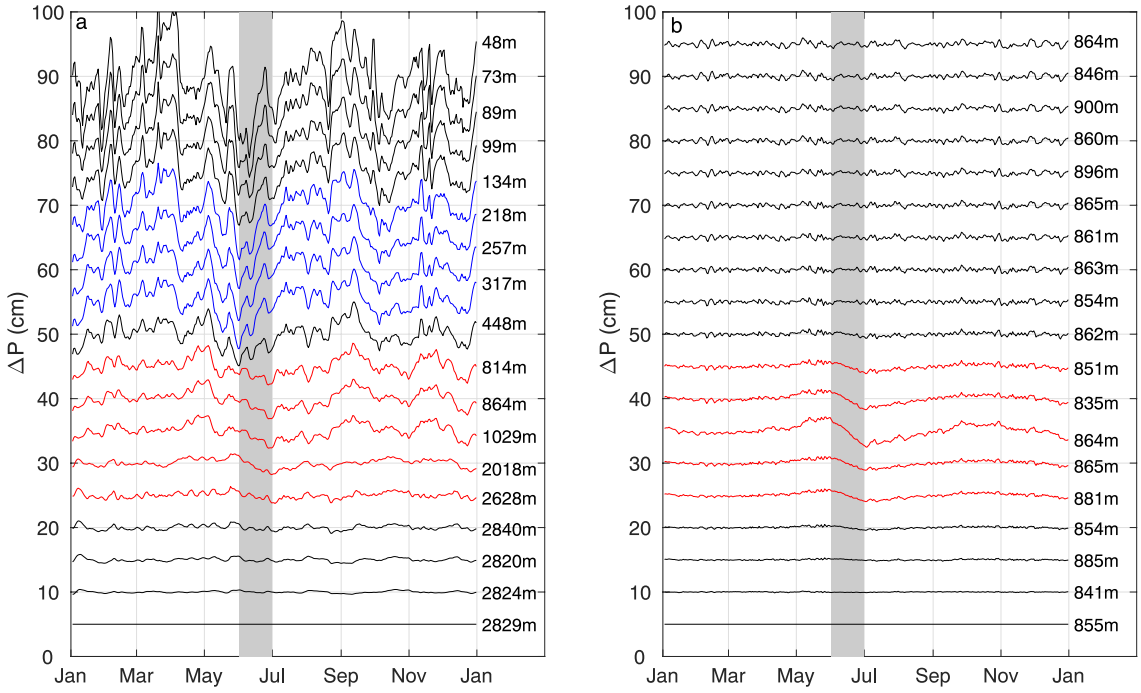

Figure S6. As for Figure 9, but for a 30-day SSE. (a) As for Figure 9b. (b) As for Figure 9c.

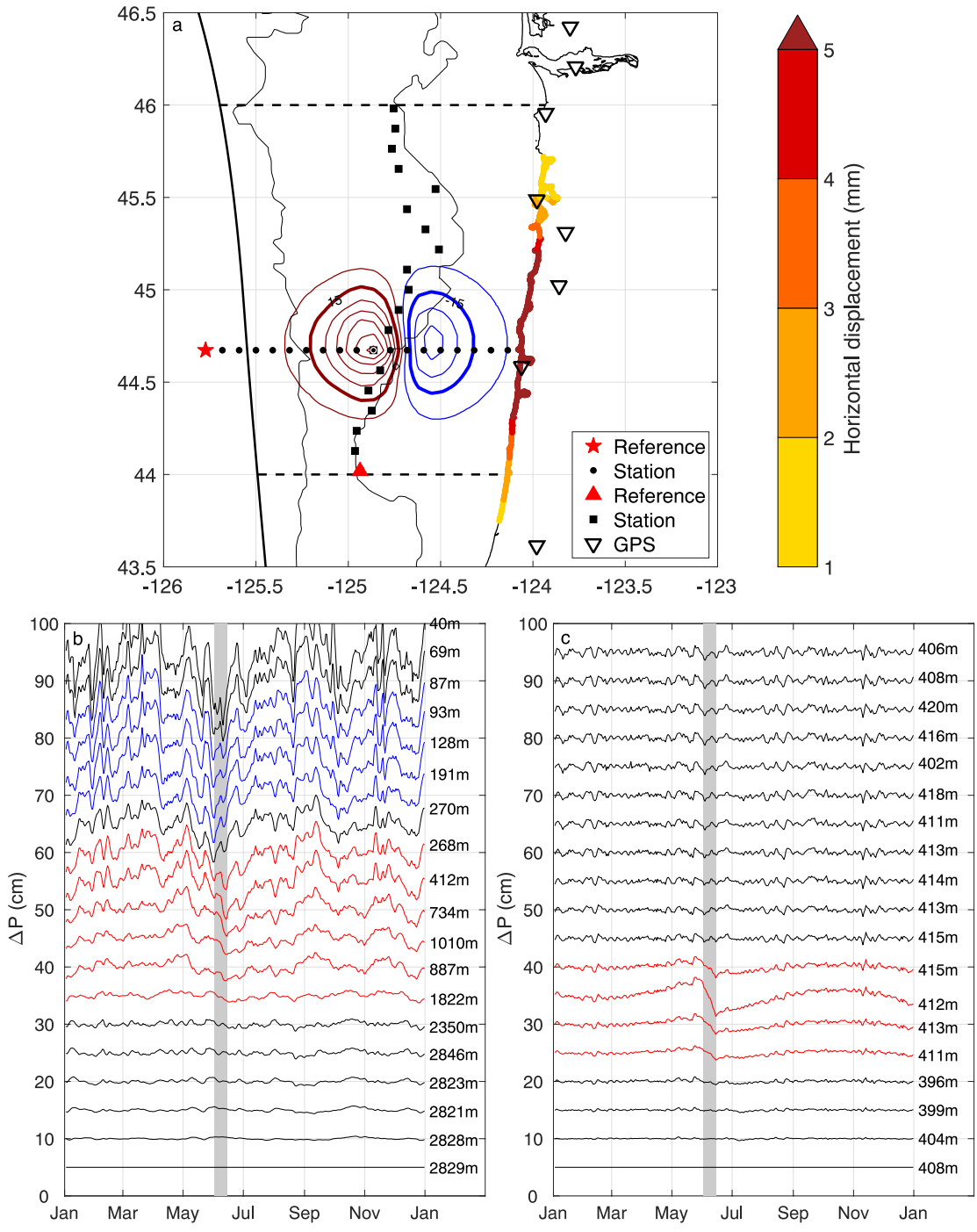

Figure S7. As for Figure 9, but for a SSE located near the shelf break.

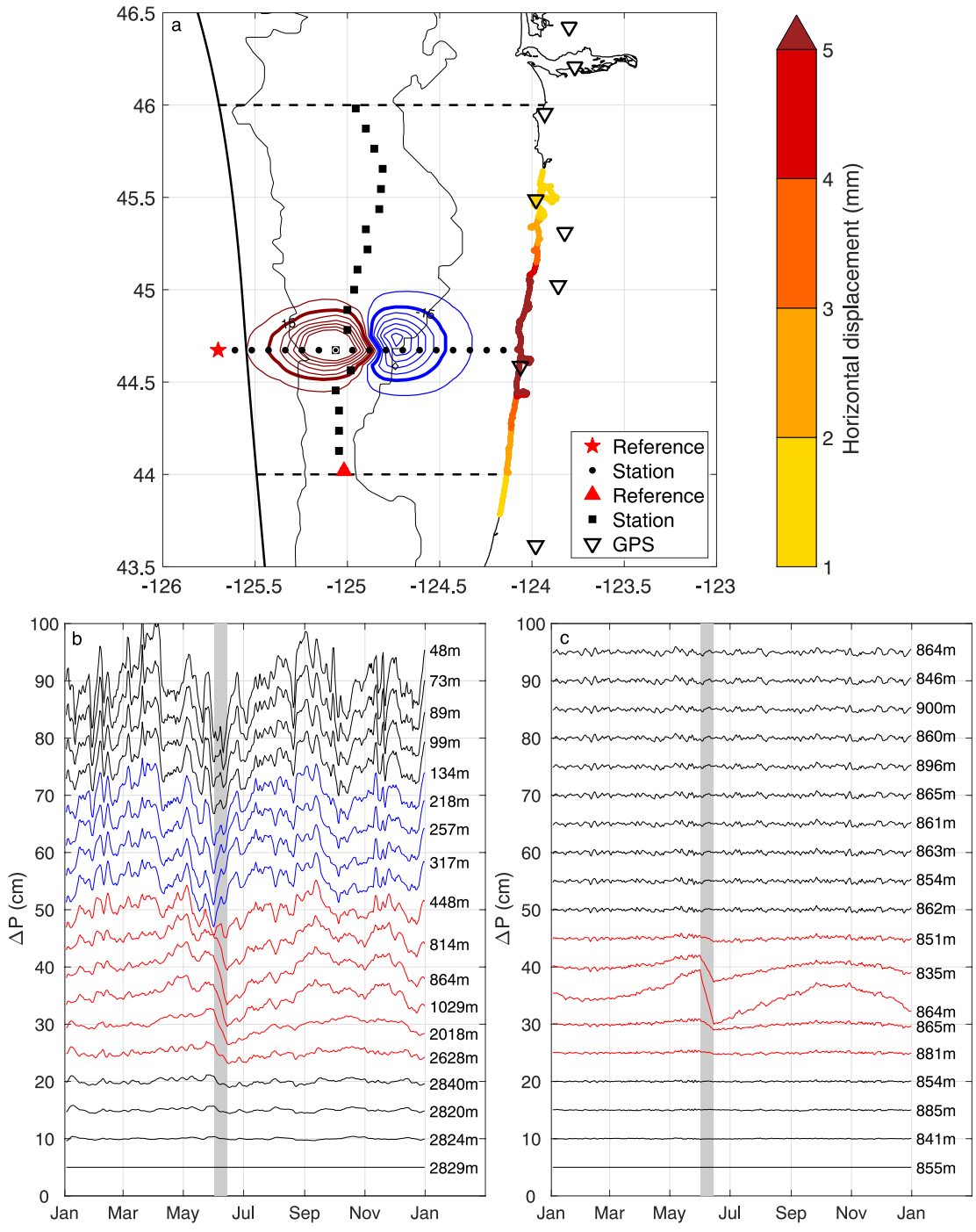

Figure S8. As for Figure 9, but for a SSE with $\Delta\sigma_E$ = 0.217 MPa ($\Delta\sigma_M$ = 0.104 MPa).

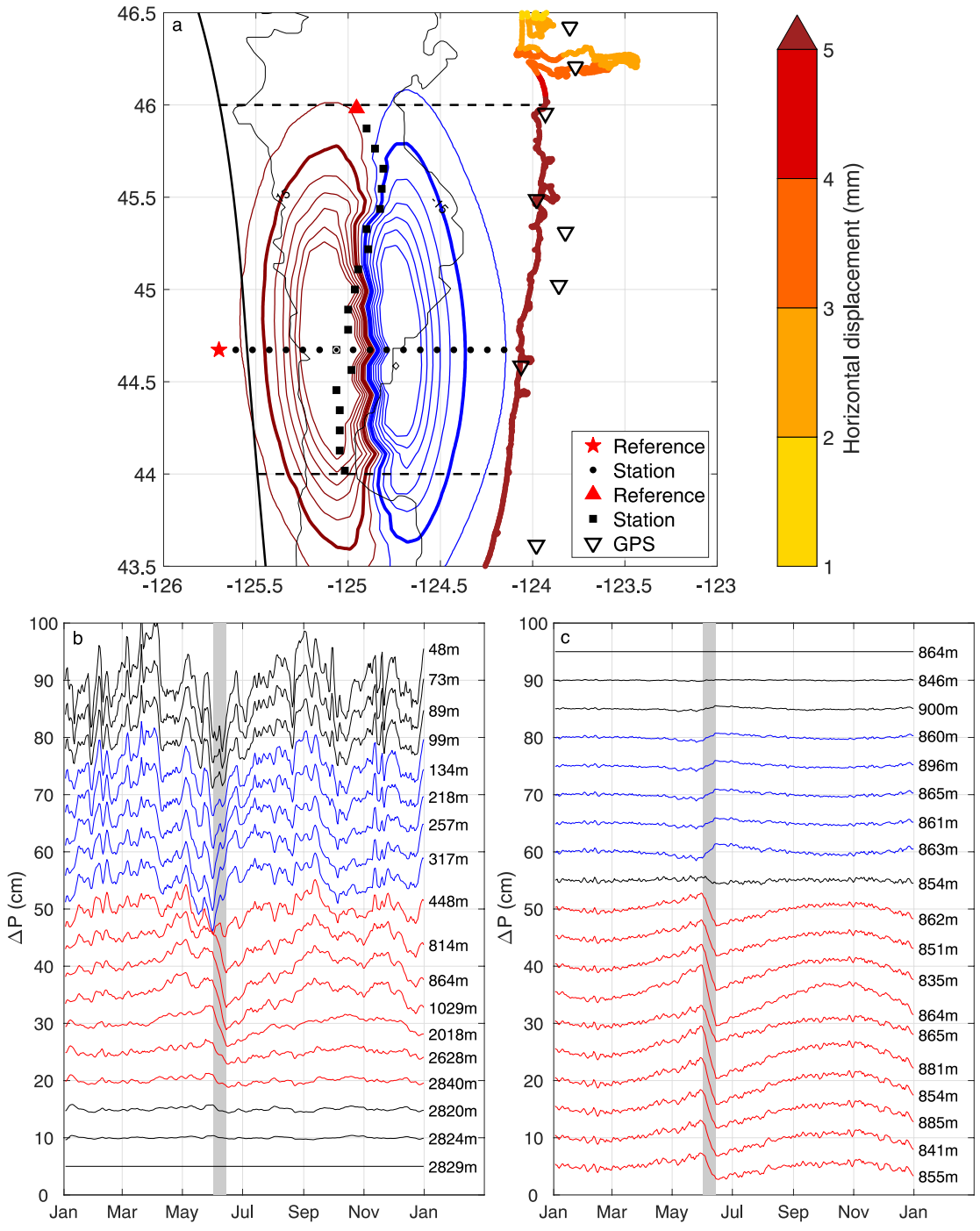

Figure S9. As for Figure 9, but for a M_w 6.9 SSE.

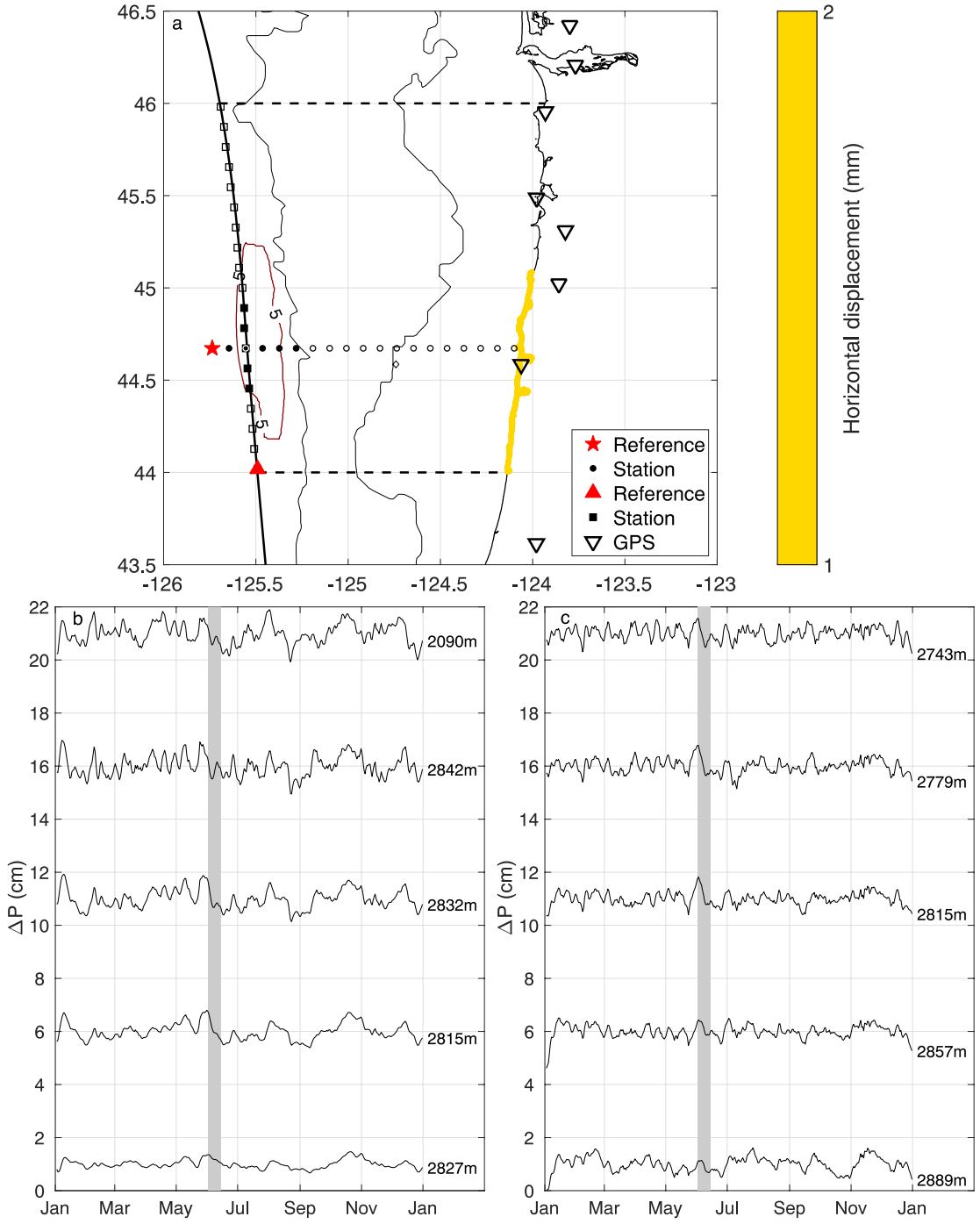

Figure S10. As for Figure 9, but for a M_w 6.2, $\Delta\sigma_E$ = 0.006 ($\Delta\sigma_M$ = 0.005 MPa) MPa SSE with 4 cm peak slip.

Table S1 Comprehensive list of depth matched differences

Depth Range	Year	Station	Depth	Depth dif.	Separation	Observations		Model		Model corrected obs.	
			z (m)	Δ z (m)	Δ xy (km)	RMS (cm)	Dif. RMS (cm)	RMS (cm)	Dif. RMS (cm)	RMS (cm)	Dif. RMS (cm)
>1400 m (Figure 5a)	2011-2012	**J26A**	**2864**	--	--	**1.5**	--	**1.3**	--	**1.6**	--
		J51A	2610	-254	244	1.7	0.8	1.4	0.4	1.9	0.8
		J34A	2574	-290	72	1.5	0.6	1.4	0.2	1.8	0.6
		J59A	2371	-493	326	1.8	0.7	1.4	0.5	1.8	0.5
		M03A	1818	-1046	363	1.7	0.7	n/a [a]	n/a [a]	n/a [a]	n/a [a]
		J42A	1540	-1810	143	1.5	0.5	1.4	0.3	1.7	0.5
		M06A	1439	-1425	106	1.5	0.7	1.4	0.4	1.6	0.6
		J51A	**2610**	--	--	**1.7**	--	**1.4**	--	**1.9**	--
		J34A	2574	-36	176	1.5	0.7	1.4	0.4	1.8	0.7
		J59A	2371	-239	81	1.8	0.5	1.4	0.3	1.8	0.5
		M03A	1818	-792	121	1.7	0.5	n/a [a]	n/a [a]	n/a [a]	n/a [a]
		J42A	1540	-1070	117	1.5	0.6	1.4	0.4	1.7	0.6
		M06A	1439	-1171	170	1.5	0.7	1.4	0.4	1.6	0.7
		J34A	**2574**	--	--	**1.5**	--	**1.4**	--	**1.8**	--
		J59A	2371	-203	257	1.8	0.7	1.4	0.5	1.8	0.6
		M03A	1818	-756	292	1.7	0.8	n/a [a]	n/a [a]	n/a [a]	n/a [a]
		J42A	1540	-1034	70	1.5	0.7	1.4	0.3	1.7	0.7
		M06A	1439	-1135	45	1.5	0.9	1.4	0.4	1.6	0.8
		J59A	**2371**	--	--	**1.8**	--	**1.4**	--	**1.8**	--
		M03A	1818	-553	48	1.7	0.4	n/a [a]	n/a [a]	n/a [a]	n/a [a]
		J42A	1540	-831	195	1.5	0.6	1.4	0.4	1.7	0.4
		M06A	1439	-932	248	1.5	0.7	1.4	0.4	1.6	0.5
		M03A	**1818**	--	--	**1.7**	--	**n/a [a]**	--	**n/a [a]**	--
		J42A	1540	-287	226	1.5	0.4	1.4	n/a [a]	1.7	n/a [a]
		M06A	1439	-379	277	1.5	0.5	1.4	n/a [a]	1.6	n/a [a]
		J42A	**1540**	--	--	**1.5**	--	**1.4**	--	**1.7**	--
		M06A	1439	-101	53	1.5	0.4	1.4	0.2	1.6	0.4

Table S2 cont.

Depth Range	Year	Station	Depth	Depth dif.	Separation	Observations		Model		Model corrected obs.	
			z (m)	Δ z (m)	Δ xy (km)	RMS (cm)	Dif. RMS (cm)	RMS (cm)	Dif. RMS (cm)	RMS (cm)	Dif. RMS (cm)
>1400 m (Figure 5a)	2012-2013	**G34B**	**2954**	--	--	**1.2**	--	**1.2**	--	**1.4**	--
		FS20B	2378	-576	241	1.3	0.5	1.2	0.3	1.4	0.5
		G26B	2357	-597	70	1.3	0.4	1.2	0.2	1.4	0.4
		FS20B	**2378**	--	--	**1.3**	--	**1.2**	--	**1.4**	--
		G26B	2357	-21	171	1.3	0.3	1.2	0.3	1.4	0.3
	2014-2015	**MJ01A**	**2908**	--	--	**1.4**	--	**2.7**	--	**2.6**	--
		O2	1909	-999	12	1.6	0.8	2.4	0.8	2.5	1.2
500 – 1400 m (Figure 5b)	2012-2013	**FS07B**	**1297**	--	--	**1.5**	--	**1.1**	--	**1.6**	--
		FS16B	1073	-224	23	1.4	0.6	1.1	0.1	1.4	0.6
		G09B	842	-455	36	1.5	0.6	1.1	0.1	1.4	0.6
		M18B	720	-577	506	1.8	1.5	1.4	0.7	1.5	1.3
		M10B	675	-622	366	1.5	1.1	1.3	0.5	1.4	1.1
		FS16B	**1073**	--	--	**1.4**	--	**1.1**	--	**1.4**	--
		G09B	842	-231	13	1.5	0.3	1.1	0.1	1.4	0.2
		M18B	720	-353	484	1.8	1.3	1.4	0.7	1.5	1.1
		M10B	675	-398	344	1.5	0.8	1.3	0.5	1.4	0.8
		G09B	**842**	--	--	**1.5**	--	**1.1**	--	**1.4**	--
		M18B	720	-122	471	1.8	1.2	1.4	0.6	1.5	1.1
		M10B	675	-167	331	1.5	0.8	1.3	0.5	1.4	0.8
		M18B	**720**	--	--	**1.8**	--	**1.4**	--	**1.5**	--
		M10B	675	-45	140	1.5	0.7	1.3	0.3	1.4	0.7
	2014-2015	**M15D**	**933**	--	--	**1.7**	--	**1.8** [b]	--	**2.1** [b]	--
		LJ01B	775	-158	263	1.6	1.0	1.9 [b]	0.4 [b]	2.0 [b]	1.0 [b]

Table S2 cont.

Depth Range	Year	Station	Depth	Depth dif.	Separation	Observations		Model		Model corrected obs.	
			z (m)	Δ z (m)	Δ xy (km)	RMS (cm)	Dif. RMS (cm)	RMS (cm)	Dif. RMS (cm)	RMS (cm)	Dif. RMS (cm)
250 – 500 m (Figure 5c)	2012-2013	**G25B**	**430**	--	--	**2.0**	--	**1.5**	--	**1.7**	--
		J33B	350	-80	354	1.9	1.3	1.7	0.9	1.6	1.4
		FS03B	345	-85	183	1.8	1.2	1.3	0.5	1.5	1.2
		J17B	286	-144	208	2.3	1.3	1.8	0.9	1.8	1.3
		J33B	**350**	--	--	**1.9**	--	**1.7**	--	**1.6**	--
		FS03B[c]	345	-5	537	1.8	1.3	1.3	1.1	1.5	1.2
		J17B	286	-64	146	2.3	0.9	1.8	0.5	1.8	0.9
		FS03B	**345**	--	--	**1.8**	--	**1.3**	--	**1.5**	--
		J17B	286	-59	391	2.3	1.7	1.8	1.2	1.8	1.4
	2014-2015	**J17D**	**285**	--	--	**2.8**	--	**1.8**	--	**2.6**	--
		J09D	252	-32	71	3.0	1.1	1.8	0.4	2.9	1.1
100 – 250 m (Figure 5d)	2011-2012	**FN08A**	**177**	--	--	**2.6**	--	**1.8**	--	**2.3**	--
		J41A	175	-2	123	3.1	1.7	2.5	1.1	2.7	1.7
		FN14A	173	-4	16	2.7	0.4	1.7	0.2	2.5	0.5
		FN07A	154	-23	8	3.3	1.0	2.5	1.0	2.5	0.6
		FN06A	134	-43	12	3.1	0.9	3.0	1.6	2.2	1.1
		J49A	120	-57	61	4.3	2.3	3.5	2.1	2.7	1.5
		J41A	**175**	--	--	**3.1**	--	**2.5**	--	**2.7**	--
		FN14A	173	-2	139	2.7	1.7	1.7	1.2	2.5	1.8
		FN07A	154	-21	118	3.3	1.8	2.5	0.8	2.5	1.7
		FN06A	134	-41	124	3.1	1.6	3.0	1.1	2.2	1.5
		J49A	120	-55	70	4.3	2.7	3.5	1.4	2.7	2.2
		FN14A	**173**	--	--	**2.7**	--	**1.7**	--	**2.5**	--
		FN07A	154	-19	23	3.3	0.9	2.5	1.1	2.5	0.6
		FN06A	134	-39	21	3.1	1.0	3.0	1.7	2.2	1.3
		J49A	120	-53	77	4.3	2.3	3.5	2.2	2.7	1.6

Table S2 cont.

Depth Range	Year	Station	Depth	Depth dif.	Separation	Observations		Model		Model corrected obs.	
			z (m)	Δ z (m)	Δ xy (km)	RMS (cm)	Dif. RMS (cm)	RMS (cm)	Dif. RMS (cm)	RMS (cm)	Dif. RMS (cm)
100 – 250 m (Figure 5d)	2011-2012	**FN07A**	**154**	--	--	**3.3**	--	**2.5**	--	**2.5**	--
		FN06A	134	-20	8	3.1	0.7	3.0	0.6	2.2	1.0
		J49A	120	-34	54	4.3	1.7	3.5	1.2	2.7	1.4
		FN06A	**134**	--	--	**3.1**	--	**3.0**	--	**2.2**	--
		J49A	120	-14	59	4.3	1.7	3.5	0.7	2.7	1.5
	2012-2013	**FS17B**	**146**	--	--	**3.0**	--	**2.1**	--	**2.1**	--
		FS11B	132	-14	15	2.7	0.9	1.6	0.9	2.2	1.2
		G17B	123	-23	83	2.9	1.0	2.4	0.6	1.9	1.0
		FS08B	120	-26	27	3.0	1.0	1.8	0.5	2.2	1.1
		FS11B	**132**	--	--	**2.7**	--	**1.6**	--	**2.2**	--
		G17B	123	-9	97	2.9	0.9	2.4	1.4	1.9	1.4
		FS08B	120	-12	14	3.0	0.6	1.8	0.5	2.2	0.7
		G17B	**123**	--	--	**2.9**	--	**2.4**	--	**1.9**	--
		FS08B	120	-3	106	3.0	0.7	1.8	1.0	2.2	1.1
	2014-2015	**FS11D**	**150**	--	--	**3.2**	--	**2.2** [b]	--	**3.1** [b]	--
		FS17D	145	-5	15	2.9	1.1	2.9 [b]	1.1 [b]	2.7 [b]	1.7 [b]
		J25D[c]	136	-14	448	3.6	2.0	3.6 [b]	2.1 [b]	4.1 [b]	2.6 [b]
		FS17D	**145**	--	--	**2.9**	--	**2.9** [b]	--	**2.7** [b]	--
		J25D[c]	136	-9	433	3.6	2.2	3.6 [b]	1.6 [b]	4.1 [b]	2.6 [b]
<100 m (Figure 5e)	2011-2012	**FN03A**	**90**	--	--	**5.3**	--	**4.2**	--	**3.4**	--
		FN19A	75	-15	21	7.1	3.8	4.8	0.8	5.2	3.8
		FN01A	54	-36	14	6.9	2.5	5.5	1.6	3.3	1.9
		FN19A	**75**	--	--	**7.1**	--	**4.8**	--	**5.2**	--
		FN01A	54	-21	17	6.9	3.5	5.5	0.9	3.3	3.5

Table S2 cont.

Depth Range	Year	Station	Depth	Depth dif.	Separation	Observations		Model		Model corrected obs.	
			z (m)	Δ z (m)	Δ xy (km)	RMS (cm)	Dif. RMS (cm)	RMS (cm)	Dif. RMS (cm)	RMS (cm)	Dif. RMS (cm)
<100 m (Figure 5e)	2012-2013	**FS19B**	**87**	--	--	**3.9**	--	**2.1**	--	**2.9**	--
		FS12B	60	-27	21	3.7	1.5	3.1	1.5	2.3	2.3
		FS15B	52	-35	15	5.8	3.7	2.9	1.3	4.5	3.4
		FS12B	**60**	--	--	**3.7**	--	**3.1**	--	**2.3**	--
		FS15B	52	-8	6	5.8	3.6	2.9	0.3	4.5	3.6
	2014-	**FS42D**	**95**	--	--	**3.5**	--	**3.3** [b]	--	**3.3** [b]	--
		FS12D	55	-40	30	4.2	1.2	3.9 [b]	0.8 [b]	4.1 [b]	1.2 [b]

Note. We include here all differences for each year within the depth bins used in Figure 5. Bold font indicates the reference against which subsequent stations were differenced ("Observations"). Values from the WCOFS model at the same locations are also included ("Model"), as are those obtained by applying the model as a correction to the data prior to differencing ("Model corrected obs."). In the 2014-2015 year, the LiveOcean model is used for those instruments within its domain, while the remainder use a truncated WCOFS model (which ends in December 2014). z – depth, xy – horizontal separation, RMS – RMS of pressure time series, Dif. RMS – RMS of difference.

[a] Model unavailable for station M03A

[b] WCOFS model available only until 12/31/2014

[c] Difference excluded from Figure 5 for display purposes